EUROPEAN ORGANIZATION FOR NUCLEAR RESEARCH

L3 Note 2774
August 16, 2002

Search for anomalous couplings in the Higgs sector at LEP

The L3 Collaboration

Abstract

We search for a Higgs particle with anomalous couplings in the $e^+e^- \rightarrow H\gamma$, $e^+e^- \rightarrow HZ$ and $e^+e^- \rightarrow He^+e^-$ processes with the L3 detector at LEP. We explore the mass range 70 GeV $< m_H <$ 190 GeV using 425 pb^{-1} of integrated luminosity at center-of-mass energies $\sqrt{s}$, ranging from 192 to 208 GeV. The Higgs decays $H \rightarrow \gamma\gamma$, $H \rightarrow Z\gamma$, and for the first time in this study $H \rightarrow WW^{(*)}$, are considered in the analysis. No evidence for anomalous Higgs production is found. These searches are combined with the results obtained at $\sqrt{s}$ = 189 GeV, using an integrated luminosity of 176 pb^{-1}, to establish limits on the anomalous couplings d and d_B, Δg_1^Z, $\Delta\kappa_\gamma$ and ξ. Limits on the $H \rightarrow \gamma\gamma$ and $H \rightarrow Z\gamma$ decay processes in the explored Higgs mass range are also obtained. All the results presented in this note are preliminary.

Submitted to the 31st *International Conference on High Energy Physics*
Amsterdam, The Netherlands 24-31 July 2002

1 Introduction

The spontaneous symmetry breaking mechanism is a fundamental ingredient of the Standard Model (SM) [1] of electroweak interactions. Despite its relevance, the experimental information on the Higgs sector of the SM is scarce and indirect at present. The search for the Higgs particle is a key issue for present and future high-energy colliders, and any deviation from expectations could be a clear guide for new physics scenarios beyond the SM.

The SM can be extended via a linear representation of the $SU(2)_L \times U(1)_Y$ symmetry breaking mechanism [2]. The lowest order representation leads to the Standard Model. At higher orders new interactions between the Higgs particle and gauge bosons become possible. They modify the production mechanisms and decay properties of the Higgs. The relevant CP-invariant Lagrangian terms for electroweak bosons are the following [3]:

$$\begin{aligned}\mathcal{L}_{\text{eff}} = g_{\mathrm{H}\gamma\gamma}\ \mathrm{H}\mathrm{A}_{\mu\nu}\mathrm{A}^{\mu\nu} \ + \ g^{(1)}_{\mathrm{HZ}\gamma}\ \mathrm{A}_{\mu\nu}\mathrm{Z}^{\mu}\partial^{\nu}\mathrm{H} \ + \ g^{(2)}_{\mathrm{HZ}\gamma}\ \mathrm{H}\mathrm{A}_{\mu\nu}\mathrm{Z}^{\mu\nu} \\ + \ g^{(1)}_{\mathrm{HZZ}}\ \mathrm{Z}_{\mu\nu}\mathrm{Z}^{\mu}\partial^{\nu}\mathrm{H} \ + \ g^{(2)}_{\mathrm{HZZ}}\ \mathrm{H}\mathrm{Z}_{\mu\nu}\mathrm{Z}^{\mu\nu} \ + \ g^{(3)}_{\mathrm{HZZ}}\ \mathrm{H}\mathrm{Z}_{\mu}\mathrm{Z}^{\mu} \\ + \ g^{(1)}_{\mathrm{HWW}}\ (\mathrm{W}^{+}_{\mu\nu}\mathrm{W}^{\mu}_{-}\partial^{\nu}\mathrm{H} \ + \ h.c.) \ + \ g^{(2)}_{\mathrm{HWW}}\ \mathrm{H}\mathrm{W}^{+}_{\mu\nu}\mathrm{W}^{\mu\nu}_{-}\end{aligned} \tag{1}$$

where A_μ, Z_μ, W_μ and H are the photon, Z, W and Higgs fields, respectively, and $\mathrm{X}_{\mu\nu} = \partial_\mu \mathrm{X}_\nu - \partial_\nu \mathrm{X}_\mu$. The couplings $g_{\mathrm{H}\gamma\gamma}$, $g^{(1)}_{\mathrm{HZ}\gamma}$, $g^{(2)}_{\mathrm{HZ}\gamma}$, $g^{(1)}_{\mathrm{HZZ}}$, $g^{(2)}_{\mathrm{HZZ}}$, $g^{(3)}_{\mathrm{HZZ}}$, $g^{(1)}_{\mathrm{HWW}}$ and $g^{(2)}_{\mathrm{HWW}}$ can be parametrized as follows [4–6]:

$$g_{\mathrm{H}\gamma\gamma} = \frac{g}{2m_{\mathrm{W}}}\ \left(d\sin^2\theta_{\mathrm{W}} + d_B\cos^2\theta_{\mathrm{W}}\right) \tag{2}$$

$$g^{(1)}_{\mathrm{HZ}\gamma} = \frac{g}{m_{\mathrm{W}}}\ \left(\Delta g_1^{\mathrm{Z}}\sin 2\theta_{\mathrm{W}} - \Delta\kappa_\gamma\tan\theta_{\mathrm{W}}\right) \tag{3}$$

$$g^{(2)}_{\mathrm{HZ}\gamma} = \frac{g}{2m_{\mathrm{W}}}\ \sin 2\theta_{\mathrm{W}}\ \left(d - d_B\right) \tag{4}$$

$$g^{(1)}_{\mathrm{HZZ}} = \frac{g}{m_{\mathrm{W}}}\ \left(\Delta g_1^{\mathrm{Z}}\cos 2\theta_{\mathrm{W}} + \Delta\kappa_\gamma\tan^2\theta_{\mathrm{W}}\right) \tag{5}$$

$$g^{(2)}_{\mathrm{HZZ}} = \frac{g}{2m_{\mathrm{W}}}\ \left(d\cos^2\theta_{\mathrm{W}} + d_B\sin^2\theta_{\mathrm{W}}\right) \tag{6}$$

$$g^{(3)}_{\mathrm{HZZ}} = \frac{g\ m_{\mathrm{W}}}{2\ \cos^2\theta_{\mathrm{W}}}\delta_{\mathrm{Z}} \tag{7}$$

$$g^{(1)}_{\mathrm{HWW}} = \frac{g\ m_{\mathrm{W}}}{m_{\mathrm{Z}}^2}\Delta g_1^{\mathrm{Z}} \tag{8}$$

$$g^{(2)}_{\mathrm{HWW}} = \frac{g}{m_{\mathrm{W}}}\frac{d}{\cos 2\theta_{\mathrm{W}}} \tag{9}$$

where g is the $\mathrm{SU(2)_L}$ coupling constant, θ_{W} is the Weinberg angle and m_{W}, m_{Z} is the W, Z mass. The five anomalous couplings d, d_B, Δg_1^{Z}, $\Delta\kappa_\gamma$ and δ_{Z} constitute a convenient set of adimensional parameters to describe deviations in Higgs-vector boson interactions. They are not severely constrained by electroweak measurements at the Z pole or low energies [3, 7]. The couplings d and d_B have been introduced in [4], while the couplings Δg_1^{Z} and $\Delta\kappa_\gamma$ are commonly used in the context of $\mathrm{e^+e^-} \to \mathrm{WW}$ studies [5]. The effect of the parameter $\xi = (1+\delta_{\mathrm{Z}})$ [6] is a global rescaling of all Higgs couplings, thus affecting the production cross sections, but not the branching fractions. Limits on this parameter can be set by a reinterpretation of our previous SM analysis [8], as shown in Figure 1, and will not be further discussed in this Note.

A typical anomalous signature would be the observation of large $\mathrm{H} \to \gamma\gamma$ and $\mathrm{H} \to \mathrm{Z}\gamma$ branching fractions, which are zero in the SM at tree level. A search for anomalous Higgs production with non-zero Δg_1^{Z} or $\Delta\kappa_\gamma$ couplings offers a complementary way to look for the same type of deviations studied in the $\mathrm{e^+e^-} \rightarrow \mathrm{WW}$ process.

The data used in this analysis have been collected with the L3 detector [9] in the center-of-mass energy range, $192 \leq \sqrt{s} \leq 208$ GeV and correspond to an integrated luminosity of 425 $\mathrm{pb^{-1}}$. Table 1 shows in more detail the integrated luminosity and the center-of-mass energies of the different data samples used.

Year	$\mathcal{L}(\mathrm{pb^{-1}})$	Average $\sqrt{s}$(GeV)
1999	28.76	192
	82.40	196
	67.59	200
	36.06	202
2000	74.66	205
	135.59	207

Table 1: Integrated luminosity and center-of-mass energies of the different data samples taken during years 1999 and 2000 and used for this analysis.

Previous experimental analyses on anomalous Higgs production accompanied by photons can be found in [10–12].

2 Analysis strategy and Monte Carlo samples

We search for a Higgs particle emitted in the $\mathrm{e^+e^-} \rightarrow \mathrm{H}\gamma$ and $\mathrm{e^+e^-} \rightarrow \mathrm{He^+e^-}$ processes at center-of-mass energies between 192 and 208 GeV. These processes are enhanced by the presence of anomalous $\mathrm{H}\gamma\gamma$ and $\mathrm{HZ}\gamma$ couplings and have sensitivity to Higgs masses up to the center-of-mass energy of the collision: $m_{\mathrm{H}} < \sqrt{s}$. The analysis is complemented with the results from L3 $\mathrm{e^+e^-} \rightarrow \mathrm{HZ}$ searches [8,13], which are sensitive to anomalous HZZ and $\mathrm{HZ}\gamma$ couplings for Higgs masses below the kinematic limit: $m_{\mathrm{H}} < \sqrt{s} - m_{\mathrm{Z}}$. All three anomalous possibilities are shown in Figure 2.

In order to search for the anomalous $\mathrm{e^+e^-} \rightarrow \mathrm{H}\gamma$ process (Figure 2a) a dedicated generator is written. It assumes the expected $(1 + \cos^2\theta_{\mathrm{H}})\ d(cos\theta_{\mathrm{H}})$ dependence for the differential cross section as a function of the Higgs production angle, θ_{H}. The generator is interfaced with the L3 simulation and reconstruction programs and takes into account initial state radiation [14] and photon emission by final-state particles [15]. The generator takes also into account spin correlations and off-shell contributions in cascade decays like $\mathrm{H} \rightarrow \mathrm{Z}\gamma \rightarrow \mathrm{f\bar{f}}\gamma$.

The $\mathrm{e^+e^-} \rightarrow \mathrm{He^+e^-}$ process (Figure 2b) is interpreted as the production of a narrow-width spin-zero resonance (the Higgs particle) in two-photon processes. For the generation of this process the PC generator [16] is used. Finally, the standard $\mathrm{e^+e^-} \rightarrow \mathrm{HZ}$ search channel is also affected by the presence of anomalous couplings (Figure 2c). The expression for the differential cross section in this case can be found in Reference [17].

For the determination of the branching fractions and partial widths of an anomalous Higgs, References [18] and [19] are used. The decay channels $\mathrm{H} \rightarrow \gamma\gamma$, $\mathrm{H} \rightarrow \mathrm{Z}\gamma$ and, for the first time the contribution from $\mathrm{H} \rightarrow \mathrm{WW^{(*)}}$, are considered for the $\mathrm{e^+e^-} \rightarrow \mathrm{H}\gamma$ process, while for the $\mathrm{e^+e^-} \rightarrow \mathrm{He^+e^-}$ production only the $\mathrm{H} \rightarrow \gamma\gamma$ mode is studied. The search is performed in the Higgs mass range 70 GeV $< m_{\mathrm{H}} <$ 190 GeV for the two-photon decay channel. For the $\mathrm{H} \rightarrow \mathrm{Z}\gamma$

channel the range of study is 95 GeV $< m_{\mathrm{H}} <$ 190 GeV. The H $\rightarrow$ WW$^{(*)}$ analysis is used in the region 130 GeV $< m_{\mathrm{H}} <$ 190 GeV.

The cases H $\rightarrow \gamma\gamma$ and H $\rightarrow$ Zγ complement each other in sensitivity, probing a large part of the parameter space. The H $\rightarrow$ b$\bar{\mathrm{b}}$ decay, considered in a previous publication [12], is dominant in the particular region where H $\rightarrow \gamma\gamma$ is strongly suppressed and H $\rightarrow$ Zγ is kinematically forbidden ($m_{\mathrm{H}} \lesssim m_{\mathrm{Z}}$), but it has not been considered in this analysis as the parameter space is, at the present center-of-mass energies, efficiently covered by the direct search e$^+$e$^-$ $\rightarrow$ HZ.

The search performed with the data taken at $\sqrt{s} = 189$ GeV (with an integrated luminosity of 176 pb^{-1}) [12] is combined with the one presented in this Note to quote combined limits on the anomalous Higgs production cross section times branching ratio of the different channels.

The analysis is performed as a function of the Higgs mass. Signal events are generated for the following Higgs masses: 70, 90, 110, 130, 150, 170 and 190 GeV. For each mass under consideration and for each process under study more than 2000 signal events are generated. For the analysis of the e$^+$e$^-$ $\rightarrow$ HZ process, we reinterpret the cross section limits obtained by L3 from SM [8] and fermiophobic [13] Higgs searches.

For the study of the SM background the following generators are considered: GGG [20] for e$^+$e$^-$ $\rightarrow \gamma\gamma(\gamma)$ events, KK2F [21] for e$^+$e$^-$ $\rightarrow$ q$\bar{\mathrm{q}}\gamma\gamma$ processes, PYTHIA [22] e$^+$e$^-$ $\rightarrow$ ZZ and e$^+$e$^-$ $\rightarrow$ Ze$^+$e$^-$ final states, KORALW [23] for e$^+$e$^-$ $\rightarrow$ WW and EXCALIBUR [24] for e$^+$e$^-$ $\rightarrow$ Weν and remaining four-fermion backgrounds.

The MC sample generated is simulated in the L3 detector and reconstructed in the same way as data. Detector inefficiencies as a function of time are taken into account.

3 Event selection

The e$^+$e$^-$ $\rightarrow$ Hγ and e$^+$e$^-$ $\rightarrow$ He$^+$e$^-$ Higgs production mechanisms lead to characteristic topologies. In an e$^+$e$^-$ $\rightarrow$ Hγ process a high-energy photon of fixed energy is produced, and typically most of the collision energy is visible in the final state. Events originating from a two-photon collision, e$^+$e$^-$ $\rightarrow$ He$^+$e$^-$, have missing longitudinal momentum and missing mass, as the two emerging electrons tend to escape detection at very low polar angles. The analysis is performed in Higgs mass steps of 1 GeV by interpolation of the generated Higgs signal efficiencies. This is particularly relevant in the case of photonic Higgs decays, where the good energy resolution of the L3 detector can be exploited efficiently.

A basic ingredient in the study is photon identification. In all analyses a photon candidate is defined as a shower in the electromagnetic calorimeter with a profile consistent with that of a photon (more than 90% of its energy contained in a 3×3 crystal matrix) and with no associated track in the vertex chamber. In addition, all photon candidates must satisfy $E_\gamma > 5$ GeV and $16° < \theta_\gamma < 164°$, where E_γ is the photon energy and θ_γ is its polar angle. These cuts reduce the background associated to initial and final-state radiation, while keeping a large efficiency for the Higgs signal.

The statistical treatment is common to all selections. Data samples are assumed to follow a Poisson distribution, according to the expected background and the signal hypothesis under consideration. All quoted limits are determined following a Bayesian approach and assuming a flat prior distribution for the signal cross section.

3.1 $e^+e^- \to H\gamma \to \gamma\gamma\gamma$ analysis

In order to select $e^+e^- \to H\gamma \to \gamma\gamma\gamma$ events we require three photon candidates in the event with a total electromagnetic energy larger than $\sqrt{s}/2$. In addition, the invariant mass of (at least) one of the photon pairs in the event, $M_{\gamma\gamma}$, must be consistent with the Higgs mass hypothesis: $\mid M_{\gamma\gamma} - m_{\mathrm{H}} \mid < 0.05\ m_{\mathrm{H}}$, with m_{H} expressed in GeV.

After these cuts the contamination from processes other than $e^+e^- \to \gamma\gamma(\gamma)$, as estimated from MC simulations, is found to be negligible. In Figure 3a the distribution of the two-photon invariant mass in data and in MC for a Higgs mass hypotheses $m_{\mathrm{H}} = 130$ GeV and a reference cross-section $\sigma_{ref} = 0.5$ pb, at $\sqrt{s} = 196$ GeV is shown.

The signal acceptance in the full phase space is determined to be in the range $35 - 45\%$, depending on the Higgs mass hypothesis and center-of-mass energy considered. The total number of expected and observed events for several Higgs mass hypotheses and for the full sample, $\sqrt{s} = 192 - 208$ GeV, are shown in Table 2, together with the limit on $\sigma(e^+e^- \to H\gamma)\ \mathrm{Br}(H \to \gamma\gamma)$ at the 95% confidence level (CL) for the average center-of-mass energy, $< \sqrt{s} >= 198$ GeV [1]. No evidence for any anomalous signal is observed, leading to the limits shown in Figure 4.

m_{H} (GeV)	Data events	Background events	95% CL Upper Limit on $\sigma(e^+e^- \to H\gamma)\ \mathrm{Br}(H \to \gamma\gamma)$ (fb)
70	6	8.6	24.7
90	13	8.4	52.7
110	9	7.7	36.7
130	6	7.0	27.7
150	7	10.5	26.4
170	21	20.8	48.7
190	23	31.9	56.5

Table 2: Number of selected candidates, background events and 95% CL cross section limits after the $e^+e^- \to H\gamma \to \gamma\gamma\gamma$ selection for different Higgs mass hypotheses for all center-of-mass energies, 192 GeV $< \sqrt{s} <$ 208 GeV.

3.2 $e^+e^- \to He^+e^-$, $H \to \gamma\gamma$ analysis

The selection of the $e^+e^- \to He^+e^-$, $H \to \gamma\gamma$ signal requires the presence of two photon candidates in the event. In addition, a kinematic fit to the signal hypothesis is performed. We assume that all the energy-momentum is lost in the beam pipe and that the visible mass of the event is consistent with m_{H} within the experimental uncertainties. Finally the χ^2 of the fit is required to be less than $50 - 0.2\ m_{\mathrm{H}}$, where m_{H} is expressed in GeV.

The distributions of the two photon invariant mass for data and MC after the kinematic fit at $\sqrt{s} = 207$ GeV are shown in Figure 3b for the Higgs mass hypothesis $m_{\mathrm{H}} = 130$ GeV. The background is dominated by $e^+e^- \to \gamma\gamma(\gamma)$ events. Since $\sigma(e^+e^- \to He^+e^-)$ is proportional to

[1] Throughout this Note, cross section measurements $\sigma(\sqrt{s})$ are combined uner the assumption of a dependence via a common coupling, i.e. $\sigma(\sqrt{s}) = \kappa\ \sigma^{SM}(\sqrt{s})$, where $\sigma^{SM}(\sqrt{s})$ the SM production cross section and κ is the common coupling, independent of $\sqrt{s}$. The average center-of-mass energy, $< \sqrt{s} >= 198$ GeV, corresponds to the luminosity weighted average value of the data sample, and is used as reference.

the partial Higgs width into photons, $\Gamma(\mathrm{H} \rightarrow \gamma\gamma)$, the limits to the cross section of the process are directly interpreted in terms of $\Gamma(\mathrm{H} \rightarrow \gamma\gamma)\ \mathrm{Br}(\mathrm{H} \rightarrow \gamma\gamma)$.

The signal acceptance in the full phase space is approximately 25%, with a smooth dependence on the Higgs mass hypothesis and the center-of-mass energy considered. The number of expected and observed events in the $\sqrt{s} = 192 - 208$ GeV range and the 95% CL limit on $\Gamma(\mathrm{H} \rightarrow \gamma\gamma)\ \mathrm{Br}(\mathrm{H} \rightarrow \gamma\gamma)$ are shown in Table 3 for several Higgs mass hypotheses. There is no evidence for any anomalous signal, leading to the limits shown in Figure 6.

$\mathrm{m_H}$ (GeV)	Data events	Background events	95% CL Upper Limit on $\Gamma(\mathrm{H} \rightarrow \gamma\gamma)\ \mathrm{Br}(\mathrm{H} \rightarrow \gamma\gamma)$ (MeV)
70	0	0.0	0.1
90	4	0.8	0.9
110	5	1.6	2.0
130	5	6.4	3.5
150	11	11.3	10.7
170	20	25.4	30.7
190	23	28.4	226.6

Table 3: Number of selected candidates, background events and 95% CL limits on $\Gamma(\mathrm{H} \rightarrow \gamma\gamma)\ \mathrm{Br}(\mathrm{H} \rightarrow \gamma\gamma)$ from the $\mathrm{e^+e^-} \rightarrow \mathrm{e^+e^-H} \rightarrow \mathrm{e^+e^-}\gamma\gamma$ selection for different Higgs mass hypotheses and all collected center-of-mass energies, 192 GeV $< \sqrt{s} <$ 208 GeV.

3.3 $\mathrm{e^+e^-} \rightarrow \mathrm{H}\gamma \rightarrow \mathrm{Z}\gamma\gamma$, $\mathrm{Z} \rightarrow \mathrm{q\bar{q}}$ analysis

The selection of the process $\mathrm{e^+e^-} \rightarrow \mathrm{H}\gamma \rightarrow \mathrm{Z}\gamma\gamma$, with $\mathrm{Z} \rightarrow \mathrm{q\bar{q}}$ requires high particle multiplicity and a pair of isolated high energy photons in the final state. The visible energy in the event, E_{vis}, must be consistent with the center-of-mass energy of the collision: $0.8 < E_{vis}/\sqrt{s} < 1.2$.

Events with an invariant mass recoiling to the two-photon system compatible the Z mass are preselected. Finally, the energy of one of the photons must lie within 3 GeV of the energy of the signal photon recoiling to the Higgs, at a given Higgs mass hypothesis.

The distribution of the photon energy of the selected events is shown in Figure 3c in data and in MC for a Higgs mass hypotheses $m_{\mathrm{H}} = 170$ GeV and a reference cross-section $\sigma_{ref} = 0.1$ pb, at $\sqrt{s} = 196$ GeV.

The total number of expected and observed events for several Higgs mass hypotheses are shown in Table 4, together with the limit on $\sigma(\mathrm{e^+e^-} \rightarrow \mathrm{H}\gamma)\ \mathrm{Br}(\mathrm{H} \rightarrow \mathrm{Z}\gamma)$ at the 95% confidence level (CL) for an average center-of-mass energy of $<\sqrt{s}>= 198$ GeV. No evidence for any anomalous signal is observed, leading to the limits shown in Figure 5.

3.4 $\mathrm{e^+e^-} \rightarrow \mathrm{H}\gamma \rightarrow \mathrm{WW^{(*)}}\gamma$, $\mathrm{W} \rightarrow \mathrm{q\bar{q}'}$ analysis

The selection of the process $\mathrm{e^+e^-} \rightarrow \mathrm{H}\gamma \rightarrow \mathrm{WW^{(*)}}\gamma$, with $\mathrm{W} \rightarrow \mathrm{q\bar{q}'}$ requires high particle multiplicity and a photon in the final state. All the available center-of-mass energy in the collision must be visible in the event ($0.6 < \mathrm{E}_{vis}/\sqrt{s} < 1.2$). The transverse energy imbalance must be less than 15% of the visible energy, and the longitudinal energy imbalance less than 20% of the visible energy.

m_H (GeV)	Data events	Background events	95% CL Upper Limit on $\sigma(e^+e^- \to H\gamma)$ Br$(H \to Z\gamma)$ (fb)
110	65	65.9	92.6
130	40	49.8	29.0
150	39	44.8	29.3
170	43	45.1	57.0
190	38	34.7	144.4

Table 4: Number of selected candidates, background events and 95% CL cross section limits after the $e^+e^- \to H\gamma \to Z\gamma\gamma$ selection for different Higgs mass hypotheses for all center-of-mass energies, 192 GeV $< \sqrt{s} <$ 208 GeV.

The photon must have an energy within 20 GeV of the nominal energy recoiling to a Higgs of a given mass ($E_\gamma = (s - m_H^2)/2\sqrt{s}$). If multiple photon candidates are observed, the photon whose energy is closest to the nominal recoiling energy is considered to be the recoil photon.

The rest of the event is clustered to four jets with the Durham algorithm. The separation parameter to go from 3 to 4 jets (y_{34}) must be larger than 0.0086.

A kinematic fit keeping the jet angles fixed and allowing the jet energies to vary is performed to improve the resolution on the reconstructed W mass. Total energy-momentum conservation is required.

For Higgs masses below the $2m_W$ threshold one of the W will be off-shell, its decay products having an invariant mass below the nominal W mass. In this case only the constraint that one of the invariant jet-jet masses be compatible with the W mass can be applied. The association with the best χ^2 is retained. For Higgs masses above $2m_W$ both W's are real and two constraints are included in the fit: both invariant jet-jet masses must be compatible with m_W.

For a given event, all possible associations between jets and W decay products are tried and the fit with best χ^2 is kept. Finally the χ^2 of the selected fit is required to be less than 6.0 for $m_H < 2m_W$ and less than 15.0 for $m_H > 2m_W$.

For selected events the invariant mass distribution of the four-jet system is calculated and compared to predictions of a given Higgs mass hypothesis. Figure 3d shows the reconstructed Higgs mass distribution in data and in MC for a Higgs mass hypotheses $m_H = 170$ GeV and a reference cross-section $\sigma_{ref} = 0.1$ pb, at $\sqrt{s} = 207$ GeV.

The total number of expected and observed events for several Higgs mass hypotheses are shown in Table 5, together with the limit on $\sigma(e^+e^- \to H\gamma)$ Br$(H \to WW^{(*)})$ at the 95% confidence level (CL) for the average center-of-mass energy of $<\sqrt{s}>= 198$ GeV. No evidence for any anomalous signal is observed, leading to the limits shown in Figure 7.

4 Limits on anomalous couplings

The analysis performed over the different Higgs production mechanism samples show that experimental data agree with SM predictions, thus leaving no room for a possible anomalous Higgs signal in the mass range under study. For this reason, the strategy followed is to constrain the possible values allowed for the anomalous couplings at 95% CL.

m_H (GeV)	Data events	Background events	95% CL Upper Limit on $\sigma(e^+e^- \to H\gamma)$ Br$(H \to WW^{(*)})$ (fb)
130	10	11.5	293.5
150	22	22.8	213.0
170	72	74.7	379.5
190	113	130.9	490.2

Table 5: Number of selected candidates, background events and 95% CL cross section limits after the $e^+e^- \to H\gamma \to WW^{(*)}\gamma$ selection for different Higgs mass hypotheses for all center-of-mass energies, 192 GeV $< \sqrt{s} <$ 208 GeV.

4.1 One-dimensional limits

In this section exclusion limits for each individual coupling are set as a function of the Higgs mass. Information at all center-of-mass energies, 192 GeV $\leq \sqrt{s} \leq$ 208 GeV, is combined, together with data taken at $\sqrt{s} = 189$ GeV [12], for the channels under consideration in this Note.

The exclusion limits are determined following similar criteria to the ones employed in the standard Higgs search [25]. For a given coupling Δ, a point in the (m_H, Δ) plane is considered as excluded at the 95% CL if the ratio of the confidence level for the signal+background hypothesis to the confidence level for the background-only hypothesis is less than 0.05. All couplings except for Δ are assumed to be zero.

The results for the four anomalous couplings: d, d_B, Δg_1^Z and $\Delta\kappa_\gamma$ are shown in Figures 8 and 9. In addition to the combined result obtained using all processes under study, the individual results for the most sensitive channels are also shown.

In all cases, the $e^+e^- \to HZ$ searches are enough to exclude the region $m_H \lesssim \sqrt{s} - m_Z$ for any value of the anomalous coupling. The fermiophobic $e^+e^- \to HZ, H \to \gamma\gamma$ search is sensitive at large values of d and d_B, for which there is an enhancement of the $H \to \gamma\gamma$ branching fraction. The standard search: $e^+e^- \to HZ, H \to b\bar{b}$ or $\tau^+\tau^-$ covers the region $d \approx d_B \approx 0$.

The $e^+e^- \to H\gamma \to \gamma\gamma\gamma$ and $e^+e^- \to e^+e^-H \to e^+e^-\gamma\gamma$ channels are specially sensitive if the $H\gamma\gamma$ coupling is large, i.e. when the combination $d \sin^2\theta_W + d_B \cos^2\theta_W$ is sizeable (Figure 8). On the contrary, the $e^+e^- \to H\gamma \to Z\gamma\gamma$ process has a dominant role when $H \to \gamma\gamma$ is suppressed (Figure 9). This is the case of the fits to Δg_1^Z and $\Delta\kappa_\gamma$ in the interesting Higgs mass range $m_Z < \sqrt{s} < 2m_W$. The sensitivity of the $e^+e^- \to H\gamma \to b\bar{b}\gamma$ channel would concern the region in which $H \to \gamma\gamma$ is small, the $HZ\gamma$ coupling is large and the $H \to Z\gamma$ decay is kinematically not possible. This implies limits in the range $m_H \approx m_Z$, and this region is already covered by the standard Higgs search limits.

The sensitivity of the analysis degrades rapidly when m_H approaches the $2m_W$ threshold, where the $H \to WW^{(*)}$ becomes dominant even in the presence of relatively large anomalous couplings.

4.2 Two-dimensional limits

Assuming the absence of anomalous WWZ and WWγ couplings ($\Delta g_1^Z = \Delta\kappa_\gamma = 0$), $H\gamma\gamma$ and $HZ\gamma$ couplings can be parametrized via the following subset of effective operators:

$$\mathcal{L}_{\text{eff}} = g_{H\gamma\gamma}\ HA_{\mu\nu}A^{\mu\nu}\ +\ g^{(2)}_{HZ\gamma}\ HA_{\mu\nu}Z^{\mu\nu}\ +\ h.c. \tag{10}$$

where $g_{\mathrm{H}\gamma\gamma}$ and $g^{(2)}_{\mathrm{HZ}\gamma}$ depend on the d and d_B couplings via Equations 2 and 4. These Lagrangians are used to set estimate the maximal partial widths and branching fractions allowed by L3 data. The results are presented in Figure 10 for two different Higgs masses, corresponding to the region of interest for Higgs searches at future colliders.

References

[1] S.L. Glashow, Nucl. Phys. **22** (1961) 579;
S. Weinberg, Phys. Rev. Lett. **19** (1967) 1264;
A. Salam, "Elementary Particle Theory", Ed. N. Svartholm, Stockholm, Almqvist and Wiksell (1968), 367;
P.W. Higgs, Phys. Lett. **12** (1964) 132.

[2] W. Buchmüller and D. Wyler, Nucl. Phys. **B 268**, (1986) 621;
C.J.C. Burgess and H.J. Schnitzer, Nucl. Phys. **B 228** (1983) 424;
C.N. Leung, S.T. Love and S. Rao, Z. Phys. **C 31** (1986) 433.

[3] O.J.P. Éboli *et al.*, Phys. Lett. **B 434** (1998) 340;
M.C. González-García, Int. J. Mod. Phys. **A 14** (1999) 3121.

[4] G.J. Gounaris, F.M. Renard and N.D. Vlachos, Nucl. Phys. **B 459** (1996) 51.

[5] K. Hagiwara *et al.*, Nucl. Phys. **B 282** (1987) 253.

[6] B. Grządkowski and J. Wudka, Phys. Lett. **B 364** (1995) 49.

[7] S. Alam, S. Dawson and R. Szalapski, Phys. Rev. **D 57** (1998) 1577.

[8] L3 Collaboration, P.Achard *et al.*, Phys. Lett. **B 517** 319 (2001).

[9] B.Adeva *et al.*, L3 Collaboration, Nucl. Inst. Meth. **A289** (1990) 35;
J.A.Bakken *et al.*, Nucl. Inst. Meth. **A275** (1989) 81;
O.Adriani *et al.*, Nucl. Inst. Meth. **A302** (1991) 53;
B.Adeva *et al.*, Nucl. Inst. Meth. **A323** (1992) 109;
K.Deiters *et al.*, Nucl. Inst. Meth. **A323** (1992) 162;
M.Chemarin *et al.*, Nucl. Inst. Meth. **A349** (1994) 345;
G.Basti *et al.*, Nucl. Inst. Meth. **A374** (1996) 293;
A.Adam *et al.*, Nucl. Inst. Meth. **A383** (1996) 342.

[10] DELPHI Collaboration, P. Abreu *et al.*, Phys. Lett. **B 458** (1999) 431.

[11] DELPHI Collaboration, P. Abreu *et al.*, Phys. Lett. **B 507** (2001) 89.

[12] L3 Collaboration, M. Acciarri *et al.*, Phys. Lett. **B 489** (2000) 102.

[13] L3 Collaboration, P. Achard *et al.*, Phys. Lett. **B 534** 28 (2002).

[14] F.A. Berends and R. Kleiss, Nucl. Phys. **B 260** (1985) 32.

[15] E. Barberio and Z. Wąs, Comp. Phys. Comm. **79** (1994) 291.

[16] F.L. Linde, "Charm Production in Two-Photon Collisions", Ph.D. Thesis, Rijksuniversiteit Leiden 1988.

[17] K. Hagiwara and M.L. Stong, Z. Phys. **C 62** (1994) 99.

[18] K. Hagiwara, R. Szalapski and D. Zeppenfeld, Phys. Lett. **B 318** (1993) 155.

[19] J.C. Romao and S. Andringa, Eur. Phys. J. **C7** (1999) 631.

[20] F. A. Berends and R. Kleiss, Nucl. Phys. **B 186** (1981) 22.

[21] KK2f version 4.12 is used: S. Jadach, B.F.L. Ward and Z. Wąs, Comp. Phys. Comm. **130** (2000) 260.

[22] PYTHIA version 5,722 is used: T. Sjöstrand, Preprint CERN-TH/7112/93 (1993) , revised 1995.

T. Sjöstrand, Comp. Phys. Comm. **82** (1994) 74.

[23] KORALW version 1.33 is used: M. Skrzypek *et al.*, Comp. Phys. Comm. **94** (1996) 216.

[24] EXCALIBUR version 1.11 is used: F.A. Berends, R. Pittau and R. Kleiss, Comp. Phys. Comm. **85** (1995) 437.

[25] The ALEPH, DELPHI, L3 and OPAL Collaborations and the LEP Working Group for Higgs boson Searches, CERN-EP-2000-055 (2000).

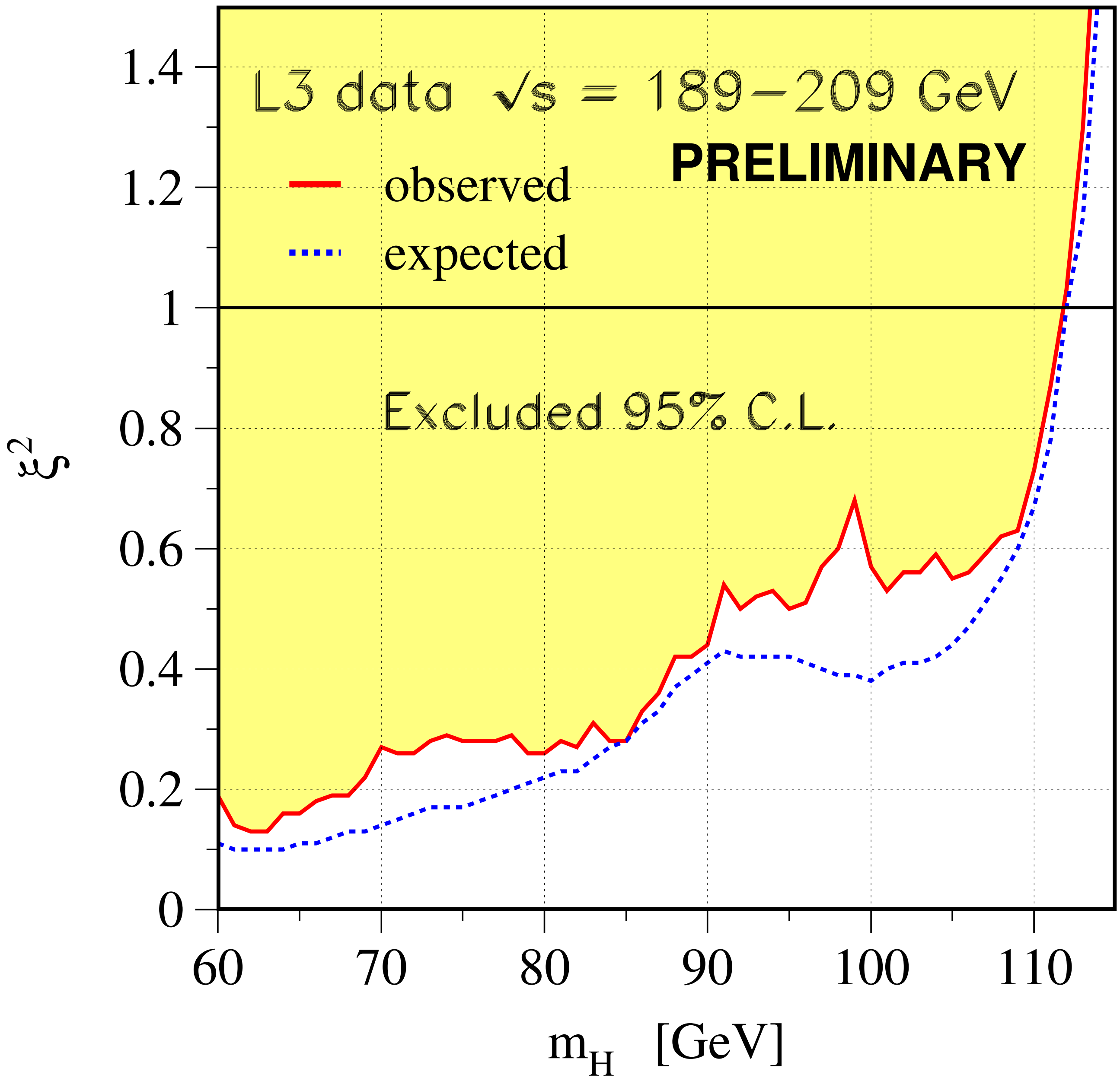

Figure 1: Excluded regions for the ξ parameter as a function of the Higgs mass hypothesis. The analysis corresponds reinterpretation of the L3 SM Higgs search analysis [8]. The SM limit, $m_{\rm H} > 112.0$ GeV, is recovered at $\xi^2 = 1$

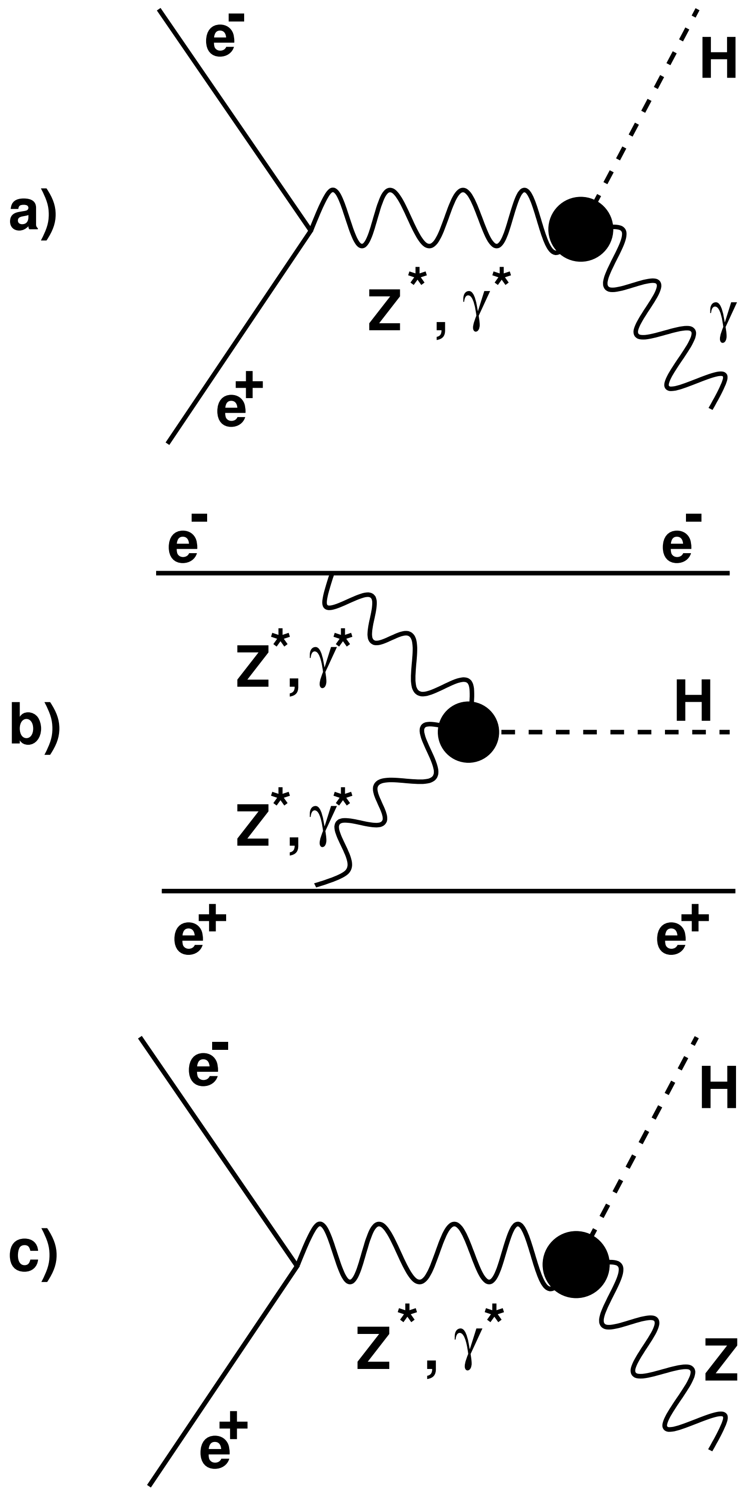

Figure 2: Relevant processes in the search for $H\gamma\gamma$, $HZ\gamma$ and HZZ anomalous couplings at LEP: a) $e^+e^- \to H\gamma$, b) $e^+e^- \to He^+e^-$ and c) $e^+e^- \to HZ$.

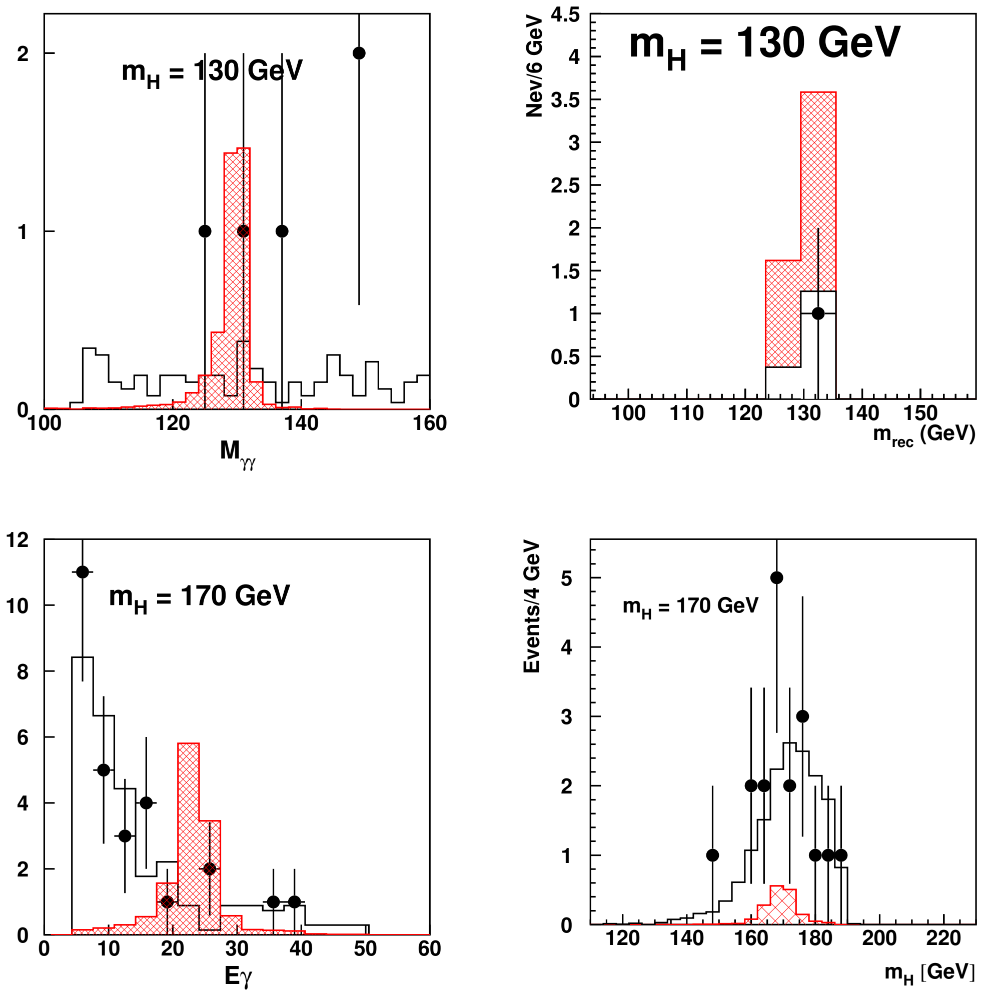

Figure 3: Selection distributions for the different Higgs search channels reported. Top-left: Reconstructed Higgs mass, M_{rec}, for $e^+e^- \to H\gamma \to \gamma\gamma\gamma$ event candidates at $m_H = 130$ GeV in data taken at $\sqrt{s} = 196$ GeV. Top-right: Reconstructed Higgs mass, M_{rec}, for $e^+e^- \to e^+e^-H \to e^+e^-\gamma\gamma$ event candidates at $m_H = 130$ GeV in data taken at $\sqrt{s} = 207$ GeV. Bottom-left: Photon energy spectrum for $e^+e^- \to H\gamma \to Z\gamma\gamma$ event candidates at $m_H = 170$ GeV in data taken at $\sqrt{s} = 196$ GeV. Bottom-right: Reconstructed Higgs mass, M_{rec}, for $e^+e^- \to H\gamma \to WW^{(*)}\gamma$ event candidates at $m_H = 170$ GeV in data taken at $\sqrt{s} = 207$ GeV. In all plots, points are data and the white histogram is the background. A Higgs signal (hatched histogram) with a cross section of 0.1 pb (0.5 pb for the $e^+e^- \to H\gamma \to Z\gamma\gamma$ channel) is also shown in the plot.

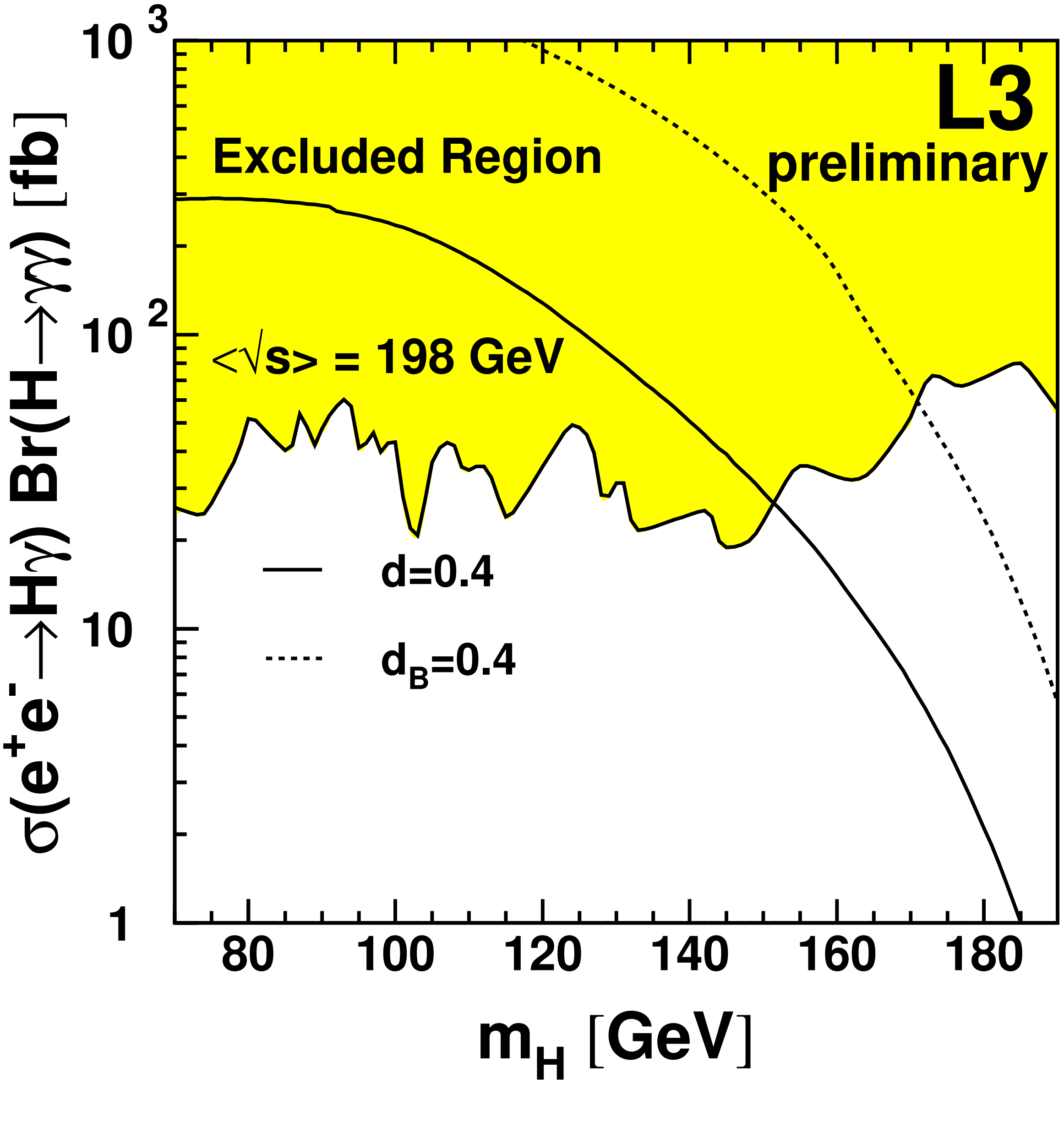

Figure 4: Cross section upper limits as a function of the Higgs mass, m_{H}, for the $\mathrm{e^+e^-} \to \mathrm{H}\gamma \to \gamma\gamma\gamma$ process in the presence of anomalous Higgs couplings at an average centre-of-mass energy, $<\sqrt{s}>= 198$ GeV.

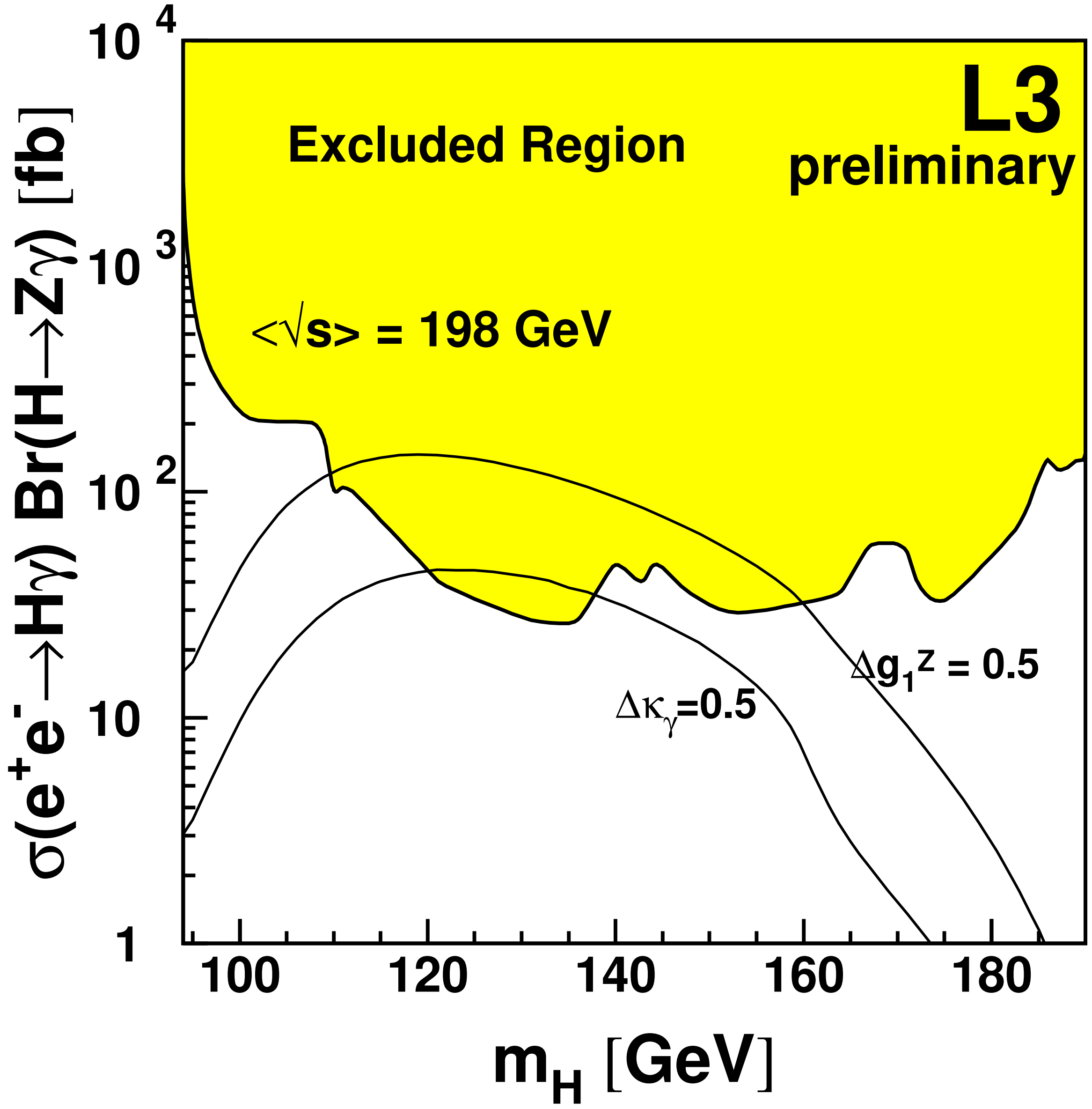

Figure 5: Cross section upper limits as a function of the Higgs mass, $m_{\rm H}$, for the $\rm e^+e^- \rightarrow H\gamma \rightarrow Z\gamma\gamma$ process in the presence of anomalous Higgs couplings at an average centre-of-mass energy, $<\sqrt{s}>= 198$ GeV.

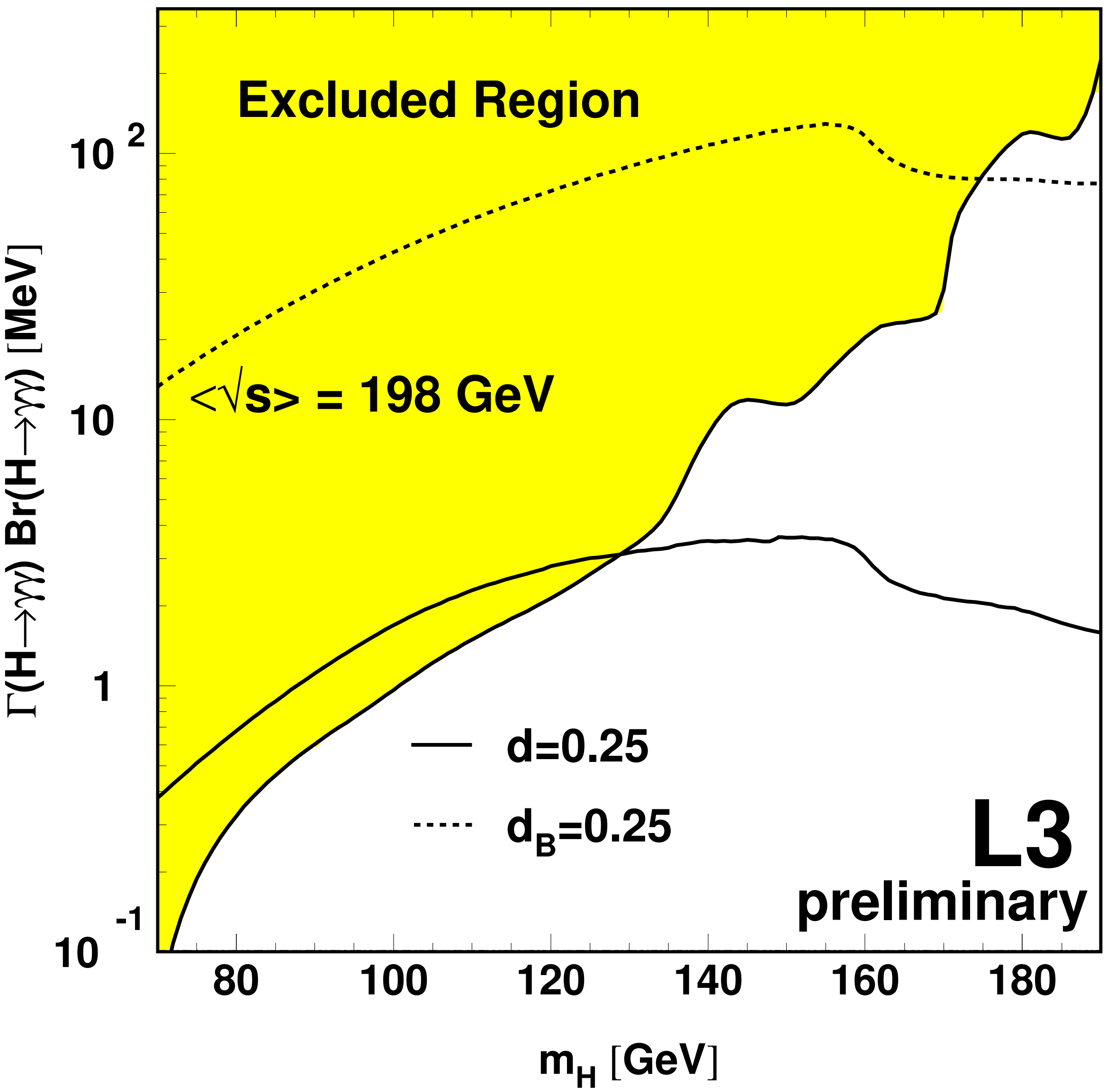

Figure 6: Upper limits on the quantity $\Gamma(\mathrm{H} \rightarrow \gamma\gamma)$ $\mathrm{Br}(\mathrm{H} \rightarrow \gamma\gamma)$ as a function of the Higgs mass, m_{H}, from the analysis of the $\mathrm{e^+e^-} \rightarrow \mathrm{He^+e^-}$ process in the presence of anomalous Higgs couplings for $\sqrt{s}$ between 192 and 208 GeV.

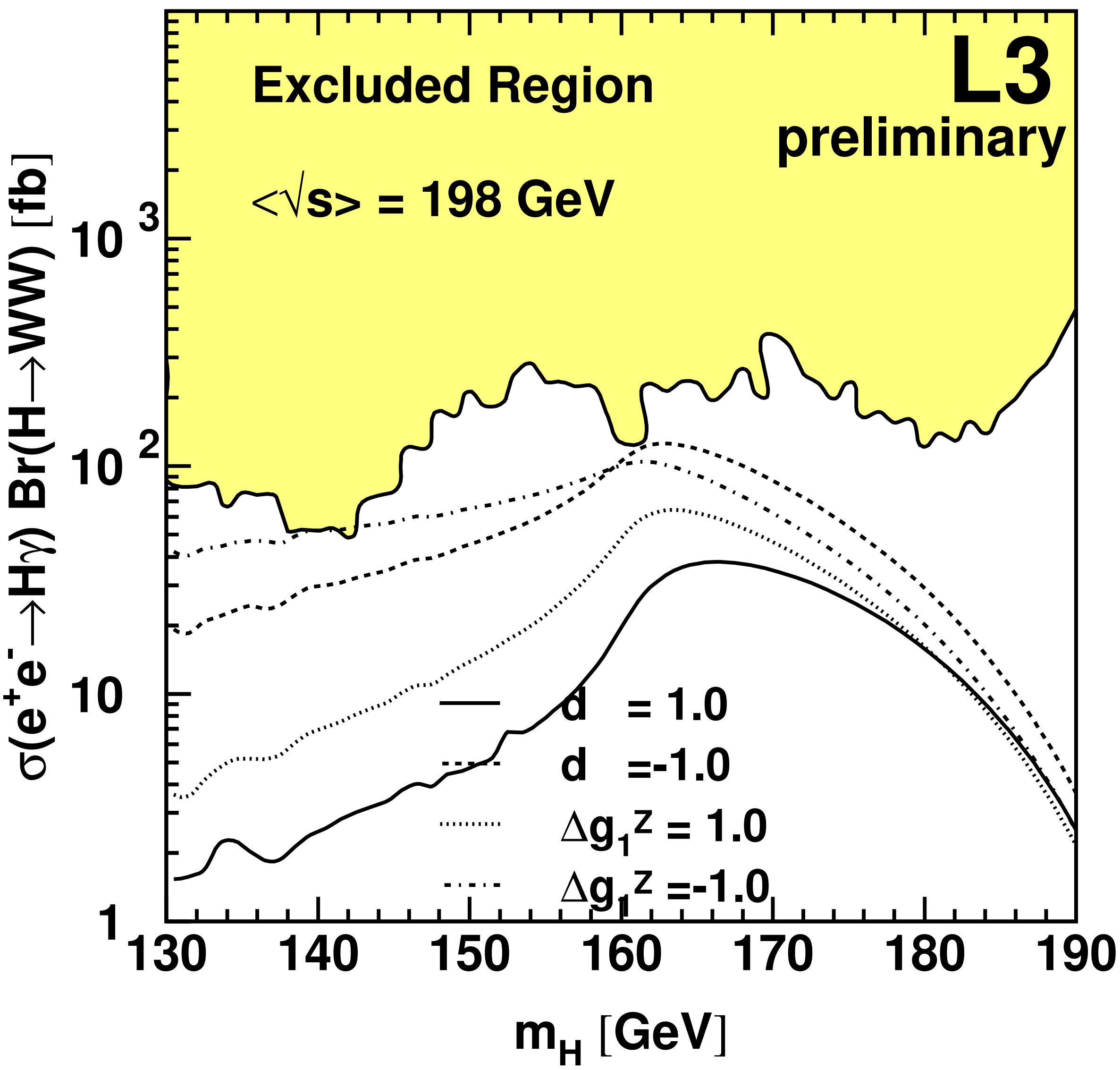

Figure 7: Cross section upper limits as a function of the Higgs mass, m_{H}, for the $\mathrm{e^+e^-} \rightarrow \mathrm{H}\gamma \rightarrow \mathrm{WW}^{(*)}\gamma$ process in the presence of anomalous Higgs couplings at an average centre-of-mass energy, $<\sqrt{s}>= 198$ GeV.

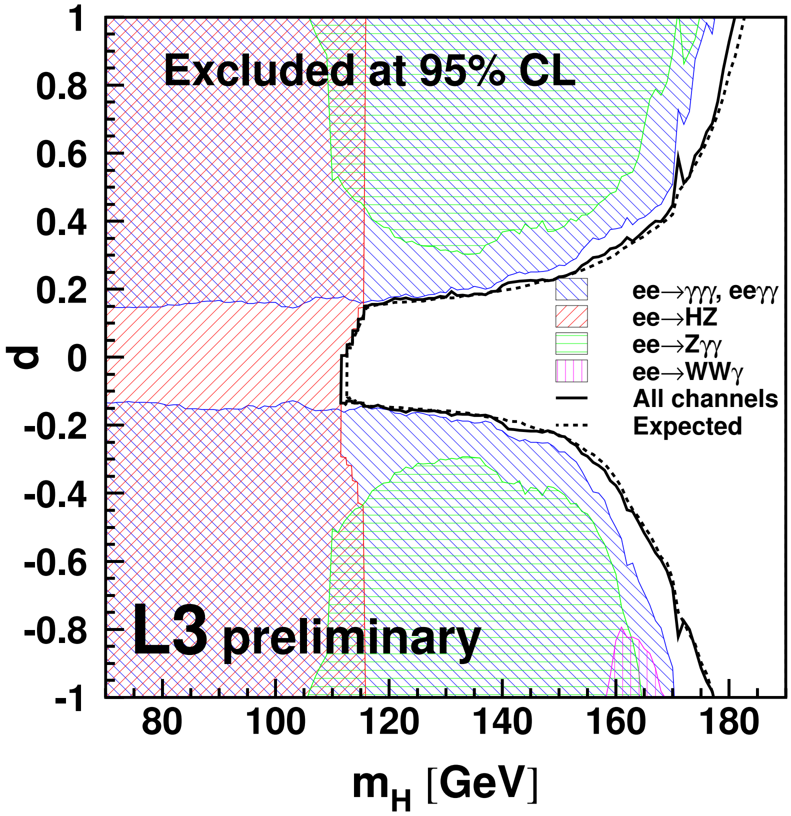

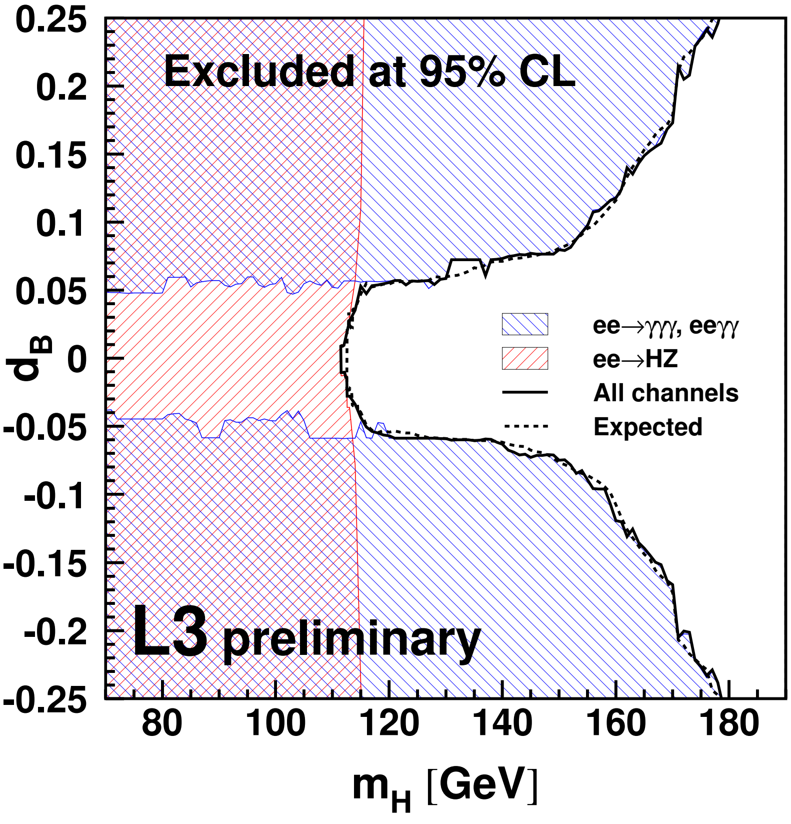

Figure 8: Excluded regions for the anomalous couplings d and d_B as a function of the Higgs mass, m_{H}. Limits on d are obtained under the assumption $d_B = \Delta g_1^{\mathrm{Z}} = \Delta\kappa_\gamma = 0$, while limits on d_B assume the relation $d = \Delta g_1^{\mathrm{Z}} = \Delta\kappa_\gamma = 0$. The different hatched regions show the limits reached by the most sensitive analyses: $\mathrm{e^+e^-} \rightarrow \mathrm{H}\gamma \rightarrow \gamma\gamma\gamma$, $\mathrm{e^+e^-} \rightarrow \mathrm{e^+e^-H} \rightarrow \mathrm{e^+e^-}\gamma\gamma$ and $\mathrm{e^+e^-} \rightarrow \mathrm{HZ}$.

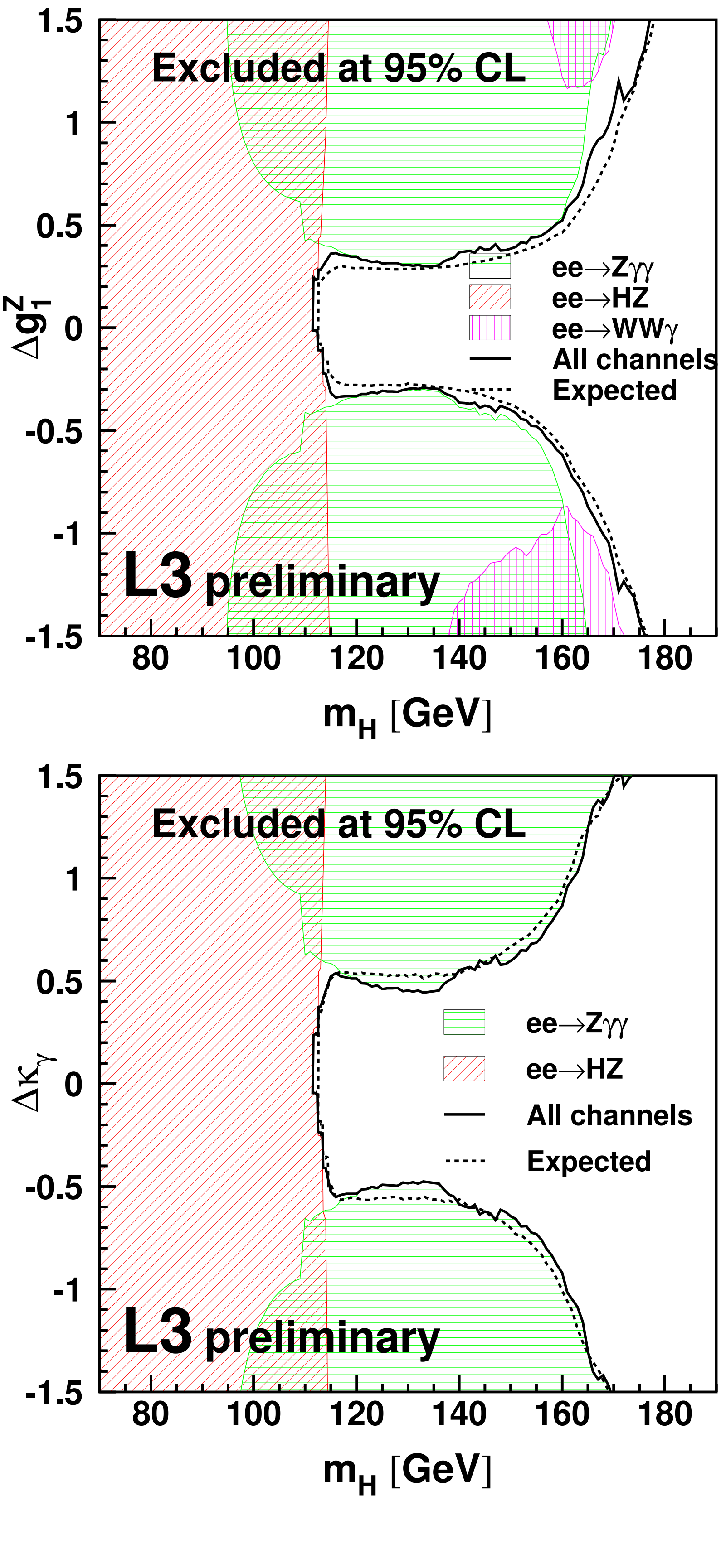

Figure 9: Excluded regions for the anomalous couplings Δg_1^{Z} and $\Delta\kappa_\gamma$ as a function of the Higgs mass, m_{H}. Limits on Δg_1^{Z} are obtained under the assumption $d = d_B = \Delta\kappa_\gamma = 0$, while limits on $\Delta\kappa_\gamma$ assume the relation $d = d_B = \Delta g_1^{\mathrm{Z}} = 0$. The different hatched regions show the limits reached by the most sensitive analyses: $\mathrm{e^+e^-} \rightarrow \mathrm{H}\gamma \rightarrow \mathrm{Z}\gamma\gamma$ and $\mathrm{e^+e^-} \rightarrow \mathrm{HZ}$.

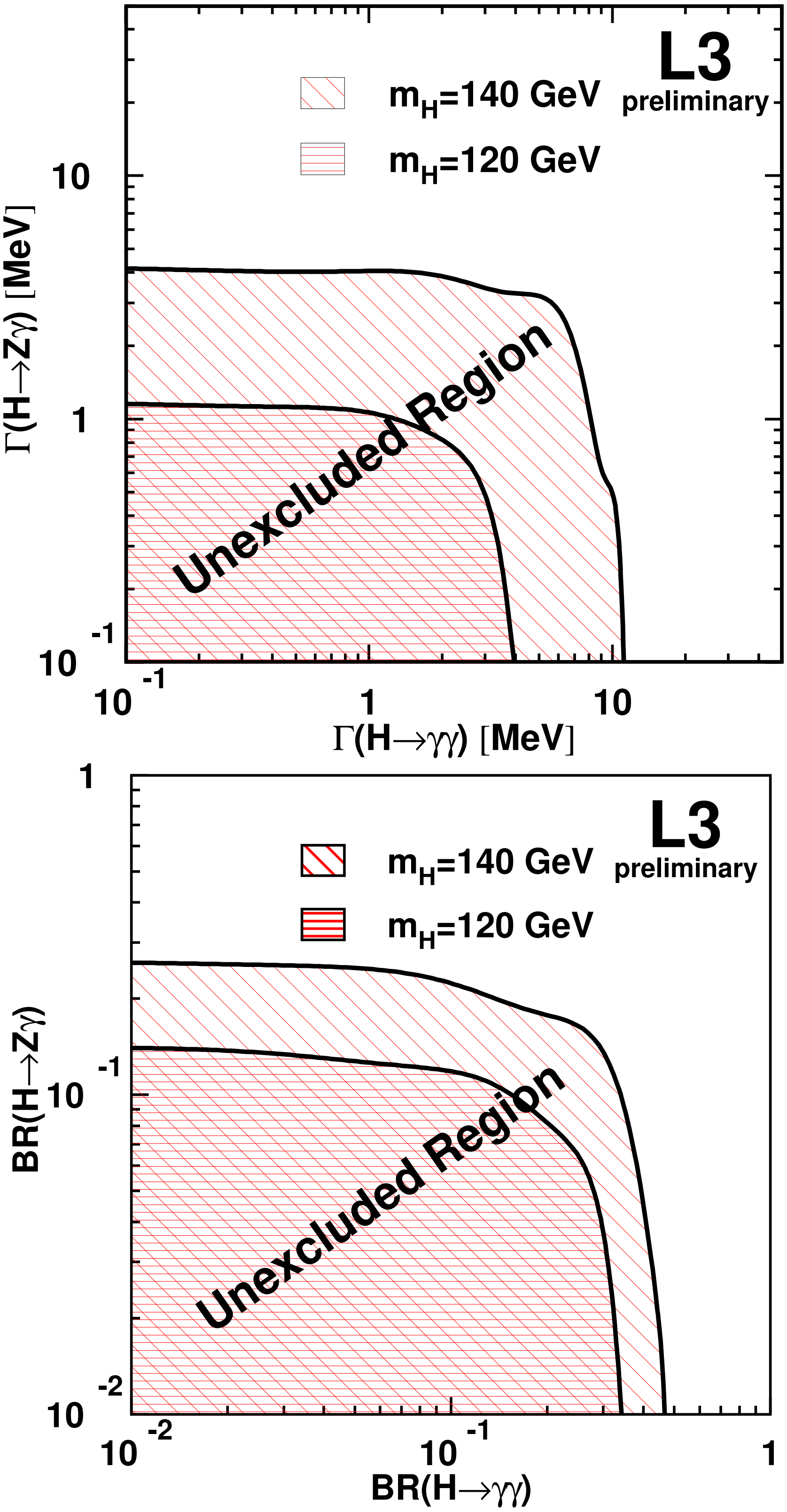

Figure 10: Unexcluded regions for the partial widths ($\Gamma(\mathrm{H} \rightarrow \gamma\gamma), \Gamma(\mathrm{H} \rightarrow \mathrm{Z}\gamma)$) and branching fractions ($BR(\mathrm{H} \rightarrow \gamma\gamma), BR(\mathrm{H} \rightarrow \mathrm{Z}\gamma)$) of the Higgs particle into $\gamma\gamma$ and $\mathrm{Z}\gamma$ final states, when d and d_B anomalous couplings are present. The contours are determined at the 95% CL for different Higgs mass assumptions. All analyzed channels are used. The results are consistent with the SM expectations ($\Gamma_{\gamma\gamma} \approx \Gamma_{\mathrm{Z}\gamma} \approx 0$).